8316 *Biochemistry* **2010,** *49,* 8316–8324
DOI: 10.1021/bi1010915

BIOCHEMISTRY
including biophysical chemistry & molecular biology
Article

Correlation of Active Site Metal Content in Human Diamine Oxidase with Trihydroxyphenylalanine Quinone Cofactor Biogenesis[†,‡]

Aaron P. McGrath,[§] Tom Caradoc-Davies,[∥] Charles A. Collyer,[§] and J. Mitchell Guss*[,§]

[§]*School of Molecular Bioscience, University of Sydney, Sydney, NSW 2006, Australia, and* [∥]*Australian Synchrotron, Clayton, Victoria, Australia*

Received July 9, 2010; Revised Manuscript Received August 13, 2010

ABSTRACT: Copper-containing amine oxidases (CAOs) require a protein-derived topaquinone cofactor (TPQ) for activity. TPQ biogenesis is a self-processing reaction requiring the presence of copper and molecular oxygen. Recombinant human diamine oxidase (hDAO) was heterologously expressed in *Drosophila* S2 cells, and analysis indicates that the purified hDAO contains substoichiometric amounts of copper and TPQ. The crystal structure of a complex of an inhibitor, aminoguanidine, and hDAO at 2.05 Å resolution shows that the aminoguanidine forms a covalent adduct with the TPQ and that the site is ~75% occupied. Aminoguanidine is a potent inhibitor of hDAO with an IC_{50} of 153 ± 9 nM. The structure indicates that the catalytic metal site, normally occupied by copper, is fully occupied. X-ray diffraction data recorded below the copper edge, between the copper and zinc edges, and above the zinc edge have been used to show that the metal site is occupied approximately 75% by copper and 25% by zinc and the formation of the TPQ cofactor is correlated with copper occupancy.

Copper amine oxidases (CAOs)[1] contain two active site cofactors that are essential for activity: a type II copper ion and a post-translationally modified tyrosine that gives rise to the redox active 2,4,5-trihydroxyphenylalanine quinone [TPQ (Figure 1A)]. CAOs catalyze the conversion of primary amines to the corresponding aldehydes in a two-step ping-pong reaction consisting of reductive and oxidative halves with the concomitant production of hydrogen peroxide and ammonia.

CAOs are found in most organisms with the exception of *Archaea*. In mammals, amine oxidases are thought to encompass a wide variety of roles, including the metabolism of reactive primary amines such as histamine, putrescine, and cadaverine (*1*) and the attachment and extravasation of leukocytes at sites of inflammation (*2*). In addition, the production of hydrogen peroxide by CAOs, long believed to be a harmful side product of the catalytic mechanism, may also play a role in cell regulation by acting as a signal-transducing molecule (*3*).

Humans have genes for three functional CAOs. AOC3 transcribes human vascular adhesion protein-1 (hVAP-1) that, in addition to its CAO activity, is a nonclassical leukocyte subtype-specific adhesion molecule. hVAP-1 is upregulated at sites of inflammation, and its amine oxidase activity has been shown to be essential for the adhesion function (*4*). AOC2 encodes retina-specific amine oxidase (hRAO) that includes a putative transmembrane domain and an enzymatic activity that is isolated to the eye (*5*). AOC1 is the gene for a diamine oxidase (DAO), an enzyme with a distinct substrate profile indicating a preference for diamines.

DAO was first identified in 1929 as histaminase, an enzyme that cleared exogenous histamine from minced lung and liver samples (*6*). Subsequently, it has become apparent that human DAO (hDAO) is the frontline enzyme for metabolizing both endogenous and exogenous histamine (*1*). The overexpression of recombinant hDAO in insect cells allowed its activity against a wide variety of substrates to be determined in vitro (*7*). These studies confirmed the preference of hDAO for diamines. In particular, two atypical diamines, histamine and 1-methylhistamine, were identified as better substrates than long aliphatic diamines such as putrescine (1,4-diaminobutane) and cadaverine (1,5-diaminopentane). hDAO has a wide tissue distribution with principal expression in the placenta (*7*), kidney (*8*), lung (*9*), and throughout the gut (*10*, *11*). hDAO has been implicated in histamine intolerance (*12*), and furthermore, it has been suggested that placental hDAO levels are indicative of a healthy pregnancy (*13*), with DAO activity increased up to 1000-fold in the blood of pregnant women (*14*). We have previously described the crystal structures of native hDAO in two crystal forms (*15*, *16*) and the structures of hDAO in complex with the noncovalent diamine inhibitors berenil [1,3-bis(4′-amidinophenyl)triazene] and pentamidine [1,5-bis(4-amidinophenoxy)pentane] (*16*).

TPQ cofactor biogenesis is a self-processing reaction requiring only the presence of the precursor tyrosine residue, molecular oxygen, and copper (*17*). To date, the exact mechanism of the acquisition of copper by CAOs is unclear. The expression of hDAO in *Drosophila* S2 cells, which lack an endogenous CAO gene, results in holoenzyme but with substoichiometric amounts of copper and TPQ (*7*). Metal ion analysis (using either ICP

[†]This research was supported by grants from the Australian Research Council (LP0669658 to C.A.C. and J.M.G.). A.P.M. was supported by an Australian Postgraduate Award for Industry.

[‡]The atomic coordinates and associated structure factors have been deposited in the Protein Data Bank as entry 3mph.

*To whom correspondence should be addressed. E-mail: mitchell.guss@sydney.edu.au. Telephone: +61-2-9351-4302. Fax: +61 2 9351 5858.

[1]Abbreviations: ABTS, 2,2′-azinobis(3-ethyl)benzthiozoline-6-sulfonic acid; AGAO, *Arthrobacter globiformis* amine oxidase; AGQ, TPQ−aminoguanidine adduct; BSAO, bovine serum amine oxidase; CAO, copper-containing amine oxidase; hDAO, human diamine oxidase; ECAO, *Escherichia coli* amine oxidase; HPAO, *Hansenula polymorpha* amine oxidase; HRP, horseradish peroxidase; PPLO, *Pichia pastoris* amine oxidase; RAO, retina-specific amine oxidase; rmsd, root-mean-square deviation; TPQ, 2,4,5-trihydroxyphenylalanine quinone; VAP-1, vascular adhesion protein-1.

 Published on Web 08/19/2010

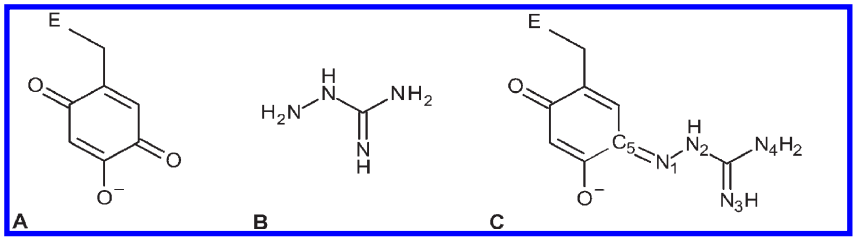

FIGURE 1: Chemical structures of (A) TPQ, (B) aminoguanidine, and (C) the TPQ−AGU adduct.

emission spectroscopy or flame atomic absorption) of recombinant hDAO expressed in *Drosophila* S2 cells has previously shown that the total content of copper and zinc, the ratio of which varies between preparations, equates to one metal per subunit of the enzyme and that the percentage of copper is approximately the same as the percentage of TPQ formation (*7*). Moreover, the presence of excess copper in either the expression media or dialysis against EDTA does not displace the more tightly bound zinc leading to stoichiometric formation of TPQ.

In previously determined crystal structures of CAOs, including that of hDAO, the TPQ can adopt one of two ordered positions or may be disordered (*18*, *19*). The TPQ can coordinate directly to the copper ion, the so-called "on-copper" conformation, in a position where it is unable to react with the substrate. Alternatively, the TPQ can be "off-copper" with its reactive quinone oxygen pointing into the active site. This off-copper orientation can be stabilized when the TPQ is reacted with a mechanism-based inhibitor, forming a covalent adduct (*20*, *21*). Furthermore, the TPQ in *Escherichia coli* amine oxidase (ECAO) has been observed as a number of intermediate species during the reductive half-reaction (*22*). In a zinc-substituted *Hansenula polymorpha* amine oxidase (HPAO) structure, the TPQ was observed as unprocessed tyrosine (*23*), with the enzyme presumably deficient for TPQ biogenesis because of the nature of the active site metal. We have explored this work further by utilizing a covalent mechanism-based inhibitor, aminoguanidine, targeted at the mature TPQ-containing enzyme in an attempt to directly correlate the amount of TPQ formed in hDAO with the relative amounts of copper and zinc bound at the active site. Aminoguanidine (Figure 1B) has long been known to be a potent inhibitor of diamine oxidases from a variety of organisms (*24*−*26*), and it is reasonable to assume that aminoguanidine will form a covalent adduct with the TPQ of hDAO. Following a similar anomalous scattering approach used to estimate the relative amounts of copper and zinc in human Cu-Zn superoxide dismutase (*27*), X-ray diffraction combined with anomalous scattering at different energies was used to estimate the amount of zinc and copper at a single site in crystals of hDAO.

EXPERIMENTAL PROCEDURES

Protein Expression, Purification, and Crystallization. hDAO was overexpressed as a secreted enzyme using the *Drosophila* S2 expression system, purified, and crystallized as described previously (*7*, *16*). In brief, hDAO crystals were grown at room temperature using the vapor diffusion method in hanging drops consisting of 2 μL of protein and 2 μL of crystallant. Crystals suitable for diffraction experiments grew within 2 weeks in 0.1 M bis-tris propane (pH 7.5), 20% (w/v) PEG3350, and 0.2 M sodium sulfate at 20 °C. Prior to the collection of multiple energy data, the crystals were transferred briefly to a drop of the crystallization mother liquor containing 30% (v/v) glycerol. Crystals of the hDAO−aminoguanidine complex were prepared by transferring hDAO crystals to a drop of the crystallization mother liquor containing 15% (v/v) MPD and 2 mM aminoguanidine and left to soak for ~2 h. Crystals were subsequently flash-cooled in a stream of dry nitrogen at 100 K prior to X-ray data collection.

hDAO Inhibition by Aminoguanidine. The concentration-dependent inhibition of hDAO by aminoguanidine was assessed by preincubation of purified hDAO (~30 nM) with aminoguanidine (3 nM to 2 μM) for 5 min before the addition of freshly prepared putrescine substrate (10 mM). Hydrogen peroxide produced during the amine oxidation reaction was monitored using a horseradish peroxidase (HRP)−2,2′-azinobis(3-ethyl)benzthiazoline-6-sulfonic acid (ABTS) coupled assay (*28*) which monitored the ABTS oxidation product that is monitored spectrophotometrically (λ_{max} = 414 nm). All assays were conducted in triplicate for each aminoguanidine concentration at 37 °C in 100 mM potassium phosphate buffer (pH 7.2) in a final assay volume of 3 mL while being stirred. An IC_{50} for aminoguanidine was calculated by fitting a sigmoidal curve to the data using the Sigmoidal Fit function in Microcal Origin (Microcal Software Inc., Northampton, MA).

hDAO−Aminoguanidine Crystal Structure. In-house data collected on the aminoguanidine-soaked hDAO crystals were recorded on a Mar345 image plate (Marresearch) using Cu Kα X-rays produced by a Rigaku RU200H rotating anode generator using Osmic optics (both from Rigaku). Data were integrated using MOSFLM (*29*) and intensities merged and scaled with SCALA (*30*).

The structure of native hDAO (*16*) [Protein Data Bank (PDB) entry 3hi7] modified for the removal of side chains of residues in the substrate channel, copper ligands, and the TPQ cofactor as well as all metal atoms and solvent molecules was used as an initial model for rigid body refinement. This was followed by multiple rounds of restrained positional and *B* factor refinement with REFMAC5 (*31*). The resulting Sigma-A-weighted electron density maps clearly showed positive difference density for the guanidinium portion of the TPQ−aminoguanidine adduct (named AGQ in the PDB entry). Between rounds of restrained refinement, the model underwent manual inspection and correction against the corresponding electron density maps in COOT (*32*). Solvent molecules were incorporated into the model as they became apparent in the electron density and were checked during refinement either manually or automatically within COOT for correct stereochemistry, sufficient supporting density above a $2F_o - F_c$ threshold of 1.0σ, and a reasonable *B* factor. Substrate channel and active site sections of the structure were modeled in a similar way in the latter stages of the refinement process with the TPQ−aminoguanidine adduct included last to ensure it was built into the density with the least bias. The restraints for the AGQ prosthetic group were generated with the assistance of the PRODRG server (*33*) in combination with manual parameter adjustment.

The quality of the model was checked intermittently for steric clashes, incorrect stereochemistry, and rotamer outliers using the MolProbity server (*34*).

Multienergy X-ray Data Collection for Metal Analysis. To quantify the relative proportions of copper and zinc at the active site, diffraction data were recorded for a native hDAO crystal at three wavelengths on the MX2 beamline of the Australian Synchrotron. A fluorescence spectrum (from 4 to 10164 eV) was recorded with an incident X-ray energy of 10159 eV, above the zinc edge, to analyze the crystal for the presence of likely anomalous scatterers. This identified the predominant metals present in the crystal as calcium, copper, and zinc, with trace amounts of iron. To maximize the anomalous scattering from zinc, a high-energy data set was collected above the zinc absorption edge at 9700 eV. In a similar fashion, a data set was collected at 9000 eV to maximize the anomalous scattering for copper that is above the copper edge but below the zinc absorption edge. A third data set below both the copper and zinc absorption edges was collected at 8800 eV. The data were integrated and scaled in HKL2000 (*35*), ensuring the preservation of intensity differences between Bijvoet pairs.

Treatment of the Multienergy X-ray Data To Determine the Relative Anomalous Scattering of Zinc and Copper. The native model of hDAO with the active site copper ligands removed was used in rigid body and then restrained refinement with diffraction data recorded at each energy. The resulting values for the calculated phases (PHIC) and their associated figure of merit (FOM) along with difference map coefficients (DELFWT and PHDELWT) were combined with the original unique reflection values using the program CAD within the CCP4 suite of programs. Anomalous difference maps were generated using FFT in CCP4, and anomalous difference peak magnitudes were tabulated. $F_o - F_c$ difference density peaks at the active site metal centers were used to scale the corresponding anomalous difference density peak magnitudes for each data set to help minimize data set variations not resulting from anomalous scattering differences.

The resulting scaled peak magnitudes for the 9700 and 9000 eV data sets were used to determine the relative anomalous scattering contributions for copper and zinc using the corresponding scattering coefficients (f'') for copper and zinc at each wavelength using the following simultaneous equations:

$$\text{scaled peak magnitude at 9700 eV} = 3.37x + 3.86y$$

$$\text{scaled peak magnitude at 9000 eV} = 3.88x + 0.55y$$

$$x = \text{copper contribution} \quad y = \text{zinc contribution}$$

The coefficients in the equations are the anomalous scattering factors (f'') for copper and zinc at the two energies (http://skuld.bmsc.washington.edu/scatter/AS_periodic.html). The metal centers in each of the two molecules in the asymmetric unit were treated independently, resulting in solutions for each of the active sites, A and B.

RESULTS

Inhibition and Structure of hDAO in a Complex with Aminoguanidine. Our kinetic analysis shows that aminoguanidine is an excellent inhibitor of recombinant hDAO with an IC_{50} of 153 ± 9 nM against putrescine oxidation. The concentration-dependent inhibition of hDAO by aminoguanidine is shown in

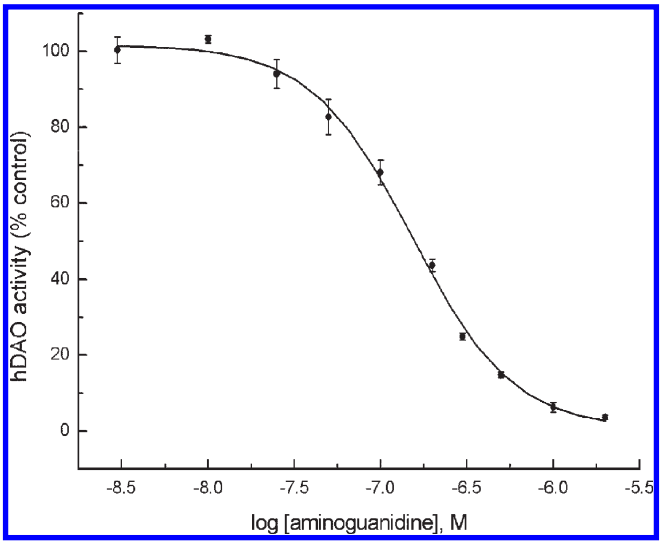

FIGURE 2: Concentration-dependent inhibition of hDAO by aminoguanidine (from 3 nM to 2 μM) against putrescine deamination. Values shown are from triplicate assays, and error bars are displayed as the standard deviation from the mean for individual replicates. An IC_{50} value of 153 ± 9 nM was determined by nonlinear regression analysis of the data.

Figure 2. X-ray crystallographic analysis confirms that aminoguanidine inhibits hDAO by the formation of a covalent link to the TPQ at the C5 position (Figures 1C and 3). This is in contrast to the previously structurally characterized inhibitor complexes of hDAO, in which the inhibitors simply bind in the active site channel without making direct interactions with the TPQ cofactor (*16*). The data processing and refinement statistics for the hDAO−aminoguanidine structure are listed in Table 1.

The structure has good refinement statistics and is very similar to the native structure, with a structural alignment of 1424 C^{α} atoms from the two structures yielding an rmsd of 0.2 Å. The only significant structural differences occur around the active site. Aminoguanidine is an irreversible inhibitor of hDAO, acting like a suicide substrate, trapping the enzyme in a covalent adduct analogous to the substrate Schiff base complex formed in the reductive half-reaction of the catalytic mechanism. The guanidine portion of the TPQ−aminoguanidine adduct is out of the plane with the phenyl ring component, indicative of the hydrazone (substrate Schiff base) adduct placing the double bond between C5 of the phenyl ring of the TPQ and N1 of aminoguanidine (Figure 1C).

The TPQ−aminoguanidine adduct makes a number of interactions within the active site (Figure 3). The oxygen of the TPQ ring makes a hydrogen bond to the hydroxyl group of Tyr359, and the carbonyl oxygen makes a hydrogen bond to a water molecule coordinated to the Cu ion. All nitrogen atoms in the guanidine group form hydrogen bonds. The nitrogen atoms, N2 and N4, form hydrogen bonds with the same carboxyl oxygen atom of the catalytic base, Asp373. In addition, N3 is hydrogen bonded to a substrate channel water molecule.

The active site type II copper ion is coordinated, as in the native structure, by the $N^{\varepsilon 2}$ atoms of the imidazole side chains of His510 and His512 and the $N^{\delta 1}$ atom of His675. In the native structure, the TPQ is on-copper and O4 of the TPQ occupies the fourth apical ligand position. In the aminoguanidine complex, the TPQ is in the off-copper conformation and a water molecule occupies the apical position in the copper coordination sphere at a distance of ~2.2 Å. At the copper site of the A chain monomer, there is some residual $F_o - F_c$ difference electron density suggesting

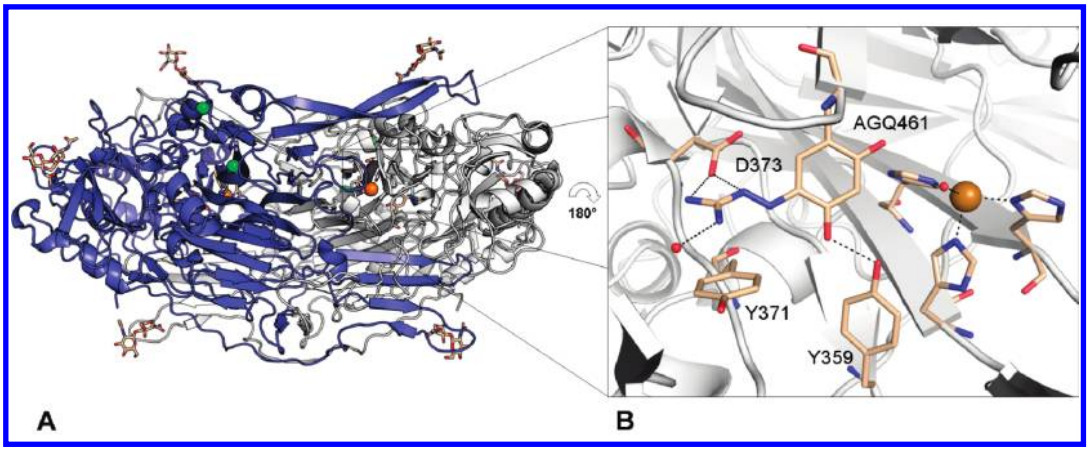

FIGURE 3: (A) Overview of the hDAO dimer and (B) zoomed in view of the TPQ−aminoguanidine (AGQ) adduct, rotated 180° with respect to panel A, formed when the TPQ cofactor reacts with aminoguanidine. (A) The two subunits of the hDAO dimer are colored blue and gray, with copper ions (orange), calcium ions (green), and active site residues and carbohydrates shown as sticks (wheat). (B) The hydrogen bond interactions of the AGQ adduct with the surrounding active site residues and solvent are shown as dashed lines.

Table 1: Diffraction Data and Refinement Statistics for the hDAO−Aminoguanidine Structure

Data Collection	
space group	$P2_12_12_1$
cell dimensions *a*, *b*, *c* (Å)	92.7, 94.6, 196.1
X-ray source	rotating anode
λ (Å)	1.5418
detector	MAR345
resolution range (Å)	31.1−2.05 (2.10−2.05)[a]
no. of observed reflections	453680
no. of unique reflections	106658
completeness (%)	95.6 (77.0)
multiplicity	4.3 (3.9)[a]
$\langle I/\sigma(I)\rangle$	10.2 (2.6)[a]
R_{merge}[b]	0.135 (0.49)[a]
R_{pim}[c]	0.071 (0.262)[a]
Refinement Statistics	
no. of reflections in the working set	101159
no. of reflections in the test set	5416
no. of protomers per asymmetric unit	2
total no. of atoms (non-H)	12719
no. of protein atoms	11537
no. of metal atoms	6
no. of water molecules	997
no. of atoms in alternate conformers	12
no. of other atoms	179
R_{cryst}	0.179 (0.277)
R_{free}	0.215 (0.310)
rmsd for bond lengths (Å)	0.009
rmsd for bond angles (deg)	1.251
$\langle B\rangle$ (Å^2)	17.84
Cruickshanks DPI[d]	0.188
PDB entry	3mph

[a]Values in parentheses are for the highest-resolution shell. [b]$R_{merge} = \sum|I_h - \langle I_h\rangle|/\sum\langle I_h\rangle$. [c]$R_{pim} = \sum_{hkl}[1/(N-1)]^{1/2}\sum_i|I_i(hkl) - \langle I(hkl)\rangle|/\sum_{hkl}\sum_i I_i(hkl)$ (*59*). [d]Diffraction Precision Indicator as output from REFMAC5 (*60*).

the presence of a second water molecule coordinating the copper ion. The electron density was not sufficiently clear to model this water. It has previously been observed that the copper water ligands in CAOs are frequently disordered or partially occupied (*19*). Similarly, some residual electron density suggests that a portion of the unprocessed Tyr461 TPQ precursor is in the on-copper conformation but was not sufficiently occupied to be included in the final model.

The occupancy of the TPQ−aminoguanidine adduct was estimated by a series of refinements with fixed partial occupancies for the atoms of the TPQ−aminoguanidine adduct other than those of the polypeptide backbone and the side chain C^β atom. The resulting $F_o - F_c$ electron density maps were manually inspected for positive and negative peaks, and the average *B* factors of the partial occupancy atoms of the aminoguanidine adduct were compared with the average *B* factors of all atoms in the model. The result is a preference for an occupancy of the aminoguanidine adduct of ~0.75 (Figure 4).

Metal Content Analysis Using X-ray Data Recorded at Different Energies. In an anomalous difference electron density map (Figure 5) calculated with the 9700 eV data (corresponding to $f''_{Cu} = 3.37$ and $f''_{Zn} = 3.86$), peaks of 45σ and 54σ occur at the copper sites in the A and B molecules, respectively (Table 2). The next four highest peaks correspond to the four calcium sites in the asymmetric unit. In a map (Figure 5) calculated with the 9000 eV data (corresponding to $f''_{Cu} = 3.88$ and $f''_{Zn} = 0.55$), anomalous difference peaks of 41σ and 47σ occur at active site metal centers A and B, respectively. The next four highest peaks again correspond with the four calcium sites in the asymmetric unit. There are no significant anomalous difference peaks at the active site metal centers in a map calculated with the 8800 eV data (corresponding to $f''_{Cu} = 0.50$ and $f''_{Zn} = 0.58$), with the four highest peaks located at the positions of the calcium ions. The scaled peak heights [(anomalous difference peak height)/($F_o - F_c$ difference peak height)] were 1.01 and 1.07 for active sites A and B at 9700 eV and 0.94 and 0.94 for active sites A and B at 9000 eV, respectively. The relative anomalous scattering contributions for copper and zinc were determined to be ~75 and ~25%, respectively (Table 3).

As mentioned above, X-ray diffraction data collected at 8800, 9000, and 9700 eV (corresponding to f''_{Ca} values of 1.10, 1.05, and 0.92, respectively) all exhibited anomalous difference peaks (data not shown) at the four sites corresponding to the calcium binding centers in the asymmetric unit. This confirms that the two putative calcium binding sites do indeed contain calcium. One of the two calcium sites in hDAO is present in all CAOs except HPAO. Interestingly, a recent report by Smith and colleagues (*36*) makes a convincing argument for the potential importance of this previously overlooked conserved calcium binding center in ECAO, with speculation that calcium at this site, although not essential, was required for maximal enzyme activity.

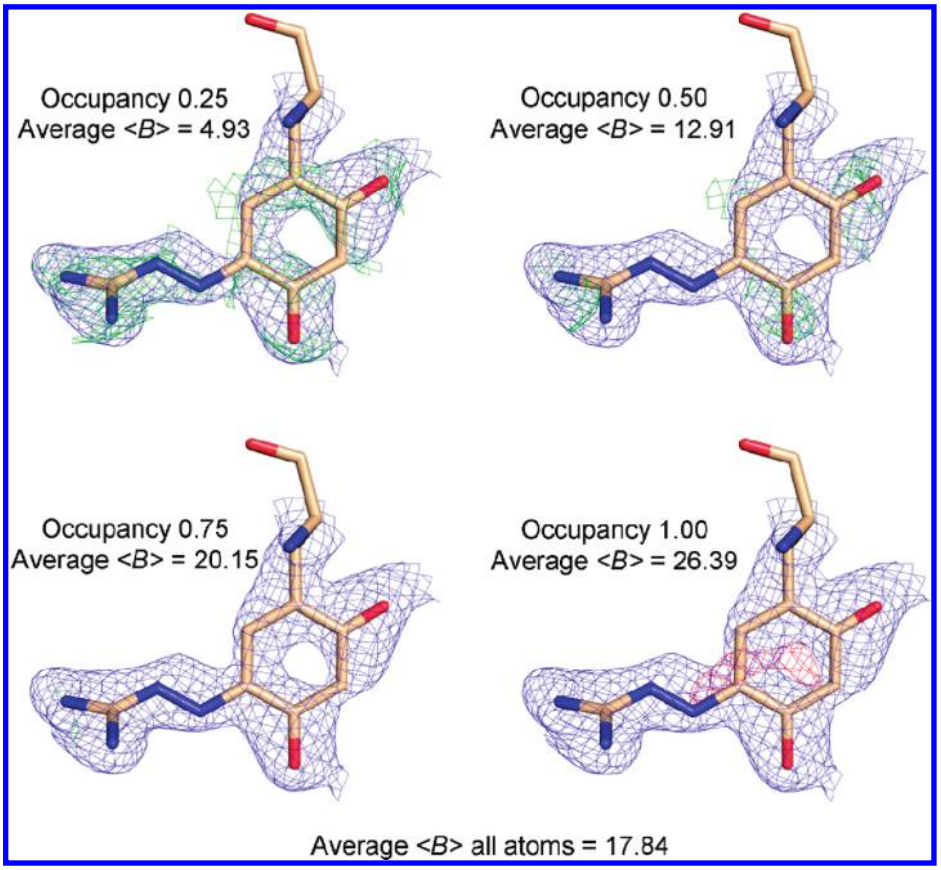

FIGURE 4: Occupancy of the TPQ−aminoguanidine adduct was estimated by a series of refinements with fixed partial occupancies for the atoms of the TPQ−aminoguanidine adduct other than those of the polypeptide backbone and the side chain C^{β} atom. The resulting electron density maps surrounding the TPQ−aminoguanidine adduct in subunit A of the model are shown as $2F_o - F_c$ at 1.0σ (blue) and $F_o - F_c$ difference density at 3.5σ and -3.5σ (green for positive and red for negative). The corresponding averaged *B* factors of the partial occupancy atoms in each case are reported for the TPQ−aminoguanidine adduct atoms in subunit A. The average *B* factor for all atoms in the model is also reported.

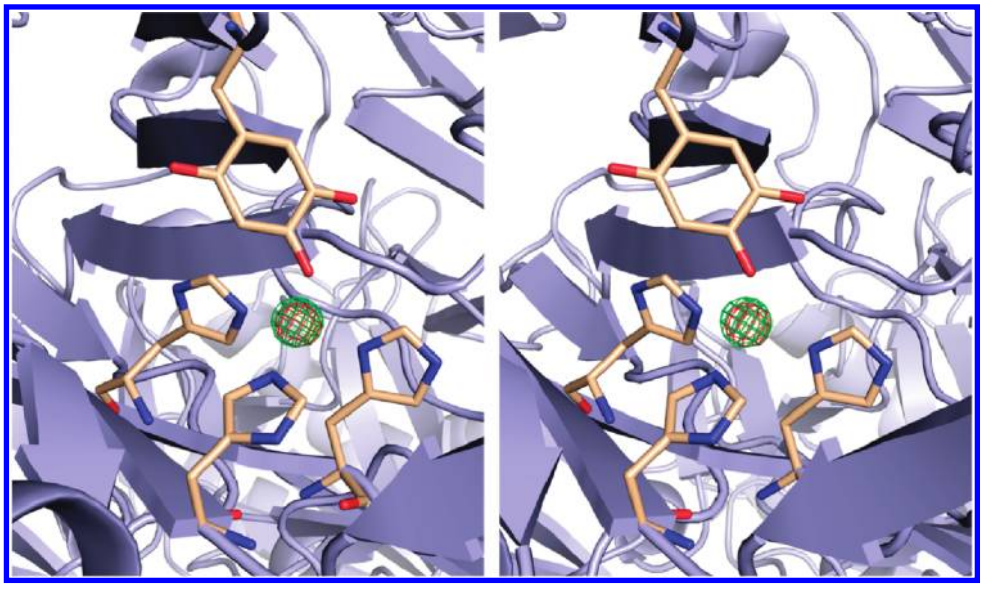

FIGURE 5: Stereoview of the anomalous difference maps calculated after removal of the copper ion from the active site of hDAO using data collected at 9700 (green) and 9000 eV (red). Both maps are shown at 30σ.

DISCUSSION

Aminoguanidine Is a Potent Irreversible Inhibitor of hDAO. This work shows that aminoguanidine is a potent inhibitor of hDAO. The adduct of TPQ and aminoguanidine has been modeled as a hydrazone, mimicking the intermediate substrate Schiff base complex formed in the reductive half-reaction of the catalytic mechanism. A hydrazone TPQ−inhibitor adduct has previously been observed for CAO inhibitors of this type (*20*, *21*). The aminoguanidine−TPQ adduct is stabilized by hydrogen bonds with the catalytic base (Asp373 in hDAO) and with a conserved active site tyrosine residue (Tyr359). The TPQ ring and guanidinium group of aminoguanidine are non-coplanar. Mure et al. (*37*)

Table 2: Anomalous Scattering Difference Peaks at the Active Site Metal Centers Scaled Relative to the Corresponding Omitted Metal $F_o - F_c$ Difference Peak Height

	9700 eV (1.278 Å)		9000 eV (1.378 Å)		8800 eV (1.409 Å)	
	metal site A	metal site B	metal site A	metal site B	metal site A	metal site B
amplitude of the metal center anomalous difference peak (height/rmsd)	45.4	54.4	40.9	47.4	6.7	3.6
amplitude of the metal center $F_o - F_c$ peak (height/rmsd)	44.9	50.9	43.6	50.4	38.3	44.8
scaled peak amplitude[a]	1.01	1.07	0.94	0.94	0.18	0.08
Cu anomalous scattering coefficient (f'')	3.37		3.88		0.50	
Zn anomalous scattering coefficient (f'')	3.86		0.55		0.58	

[a]Scaled peak heights were determined as (anomalous difference peak)/($F_o - F_c$ difference peak height).

Table 3: Anomalous Scattering Contributions from Cu and Zn at Active Site Metal Centers

	metal site A	metal site B
anomalous contribution of Cu (%)	80.18	75.68
anomalous contribution of Zn (%)	19.82	24.32

have shown that in the ECAO−2-hydrazinopyridine (2HP) complex the corresponding active site Tyr and Asp residues stabilize the adduct in the hydrazone form over the thermodynamically more favorable azo form observed in solution for a model compound. Interestingly, it was shown that the pK_a of the catalytic base aspartic acid residue in ECAO was increased to ~9.7 and that the deprotonation of the Asp resulted in the conversion of the adduct from the hydrazone to the azo tautomer (*37*). Furthermore, a Y369F mutation (corresponding to Y359 in hDAO) in ECAO resulted in the gradual conversion to a new species in which the TPQ−2HP adduct has migrated to ligate the active site Cu^{2+} (*38*). The hDAO−aminoguanidine structure reported here confirms the importance of these two residues and highlights how the active site pocket of CAOs has evolved to stabilize a specific conformation of the substrate Schiff base intermediate to optimize α-proton abstraction by the catalytic base during the reductive half-reaction.

Aminoguanidine was first reported in 1952 to be a potent inhibitor of DAO (*39*). Inhibition of human recombinant VAP-1 by aminoguanidine has an IC_{50} of ~30 μM (*40*), more than 1000-fold less potent than its inhibition of porcine kidney diamine oxidase (IC_{50} = 14.9 nM) (*41*) and 200 times less potent than the IC_{50} for hDAO reported here (~150 nM). This confirms the belief that aminoguanidine is specific for copper diamine oxidases (*41*−*44*). Aminoguanidine, an α,β-dicarbonyl scavenging agent, is an experimental therapeutic for the prevention of advanced glycation end product (AGE) formation from α,β-dicarbonyl precursors (*45*, *46*). Accumulation of irreversible AGEs, via nonenzymatic glycation of proteins, is directly implicated in the development and progression of diabetic complications such as diabetic nephropathy, a condition that can lead to end stage renal disease in patients with diabetes mellitus. Diabetic nephropathy has been described as a worldwide medical catastrophe, with the U.S. Renal Data System (USRDS) recording a continuous increase in the incidence of end stage renal disease in patients with diabetes mellitus over the past two decades (*46*). Although several clinical trials suggest that aminoguanidine treatment is therapeutically beneficial in treating patients with diabetic nephropathy, there are many reported adverse reactions to high doses of aminoguanidine, including flu-like symptoms, abnormal kidney function tests, and effects on the gastrointestinal tract (*45*−*47*). The peak plasma concentration of aminoguanidine in clinical therapy has been estimated to be ~50 μM (*45*), vastly in excess of the ~150 nM IC_{50} of hDAO and enough to inhibit the majority of peripheral VAP-1 (IC_{50} ~ 30 μM). Aminoguanidine, when administered in small doses, nevertheless remains a feasible means of treating diabetic nephropathy as well as other AGE-related disorders.

Zn^{2+} Competes with Cu^{2+} for Binding at the Active Site Metal Position. Anomalous dispersion experiments indicate that crystals of recombinant hDAO contain around ~75% copper and ~25% zinc at the active site metal position. This agrees well with independent estimates of the amount of active TPQ in the enzyme from the electron density and atomic thermal displacement factors for the TPQ−aminoguanidine adduct. This method for structurally quantifying the relative amounts of two metals at the same crystallographic position shows that Zn^{2+} competes with Cu^{2+} directly for binding at the active site and suggests that it is the Zn-bound enzyme that is unable to form the quinone cofactor. As hDAO is expressed in *Drosophila* S2 cells, which contain no gene for a TPQ-type CAO, this also has implications for the incorporation of Cu^{2+} into a heterologously expressed CAO in a zero-CAO background expression host.

At present, the mechanism for copper acquisition by CAOs is unclear (*48*). However, expression of active Cao1 (previously named SPAO1), a CAO from *Schizosaccharomyces pombe*, in *Saccharomyces cerevisiae*, one of the few yeast species that lacks an endogenous CAO, was dependent on the presence of an endogenous *S. cerevisiae* copper chaperone, metal homeostasis factor Atx1 (*49*). Indeed, more recently, this work was expanded further to also show the putative ortholog of *S. cerevisiae* Atx1 in *Sc. pombe* (which are 56% identical in sequence) participated in the delivery of copper to endogenously expressed Cao1 (*48*). As mentioned above, *Drosophila melanogaster* S2 cells, used to express recombinant hDAO in this study, also lack an endogenous TPQ-type CAO gene. However, *D. melanogaster* does express one member of the copper-containing amine oxidase family, lysyl oxidase (EC 1.4.3.13). Lysyl oxidase-type CAOs are, however, monomeric proteins containing a lysine-tyrosylquinone cofactor and have no significant sequence similarity to dimeric TPQ-type CAOs such as hDAO. A protein BLAST search of the *D. melanogaster* genome using the sequence of Atx1 from *Sc. pombe* reveals *D. melanogaster* Atox1 is 45% identical in sequence to the yeast protein. Also, a query of the human genome with Atox1 from *D. melanogaster* reveals that human copper transport protein Atox1 is 50% identical in sequence to *D. melanogaster* Atox1. It is possible that Atox1 in the *D. melanogaster* S2 cells is delivering copper to the heterologously expressed recombinant hDAO, although in a suboptimal fashion. This is a possible

explanation for the < 100% occupancy of copper seen in the active site of crystallized hDAO described in this study. It would be intriguing to see if coexpression of hDAO and human Atox1 helped improve copper loading in a non-native expression system without background CAO expression such as in *D. melanogaster* S2 cells.

Another possibility that has been suggested is that the copper and zinc content in the recombinant hDAO may be determined by the total metal ion availability in the *Drosophila* secretory pathway and the relative affinity of the active site for these two transition metals (*7*). Recombinant HPAO overexpressed in *S. cerevisiae* in a copper-deficient media was shown to have a high affinity for binding zinc and to compete with trace copper for binding. In contrast, HPAO expressed in *E. coli* in a low-copper environment resulted in apoenzyme free of both Zn and Cu (*50*). It therefore seems possible that the in vivo assembly of the same CAO in either a pro- or eukaryotic system has different mechanisms for metal ion insertion.

Zn^{2+} Is Unable To Promote TPQ Biogenesis, and Hence, Zinc-Substituted hDAO Is Also Deficient in Amine Oxidase Activity. Zn^{2+}-substituted CAOs have been shown to be minimally active or inactive (*18*), and minimal activity is thought to be most likely due to copper contamination during the reconstitution procedure. In a structure of zinc-substituted HPAO, the TPQ residue was observed as unprocessed tyrosine (*23*). Furthermore, HPAO expressed in a heterologous *S. cerevisiae* expression system under different culturing conditions led to the incorporation of varying amounts of zinc-bound CAO, and zinc−copper CAO heterodimers were correlated with the incapacity for rapid substrate turnover (*51*). In other words, zinc-substituted HPAO not only was deficient for TPQ biogenesis but also was observed to inhibit amine oxidase activity at adjacent copper-containing subunits in zinc−copper heterodimers. The TPQ-less precursor AGAO enzyme incubated with various divalent metal ions indicated that Co^{2+}, Ni^{2+}, and Zn^{2+} bound tightly to the active site and were not displaced by the addition of excess Cu^{2+} (*52*). Furthermore, addition of pure O_2 gas to Co^{2+}- and Ni^{2+}-containing AGAO solutions exhibited TPQ production, although much less efficiently than in the presence of Cu^{2+}. It is unlikely that either Co^{2+} or Ni^{2+} is relevant for TPQ biogenesis in vivo. Zn^{2+} therefore has a high affinity for the active site in CAOs but will not promote TPQ biogenesis or be displaced by Cu^{2+} when the latter is added in excess.

A refined consensus mechanism for Cu^{2+}-dependent TPQ generation has emerged (*53*). Central to this mechanism are spectroscopic observations for another eukaryotic CAO, HPAO, indicating that the precursor tyrosine is activated for reaction with dioxygen by binding to Cu^{2+} in a ligand-to-metal charge transfer complex (*54*, *55*). The inability of zinc to promote TPQ biogenesis indicates a key redox role for copper in promoting this reaction with dioxygen. This mechanism is further substantiated by TPQ biogenesis intermediates observed crystallographically in AGAO (*56*, *57*).

We have sought to directly correlate the amount of copper and zinc at the active site with the presence and absence of TPQ, respectively. Our observation that a complex is formed only between hDAO and aminoguanidine (*in crystallo* via a substrate Schiff base complex with the mature TPQ cofactor) at the same ratio as the copper content at the active site (as determined via anomalous diffraction metal quantification experiments *in crystallo*) shows that this is indeed the case.

Comparisons drawn between cofactor biogenesis and substrate catalysis by CAOs by Klinman and colleagues (*55*, *58*) highlight the requirement to utilize a single transition metal to conduct several reactions at a single reaction site. The optimal metal must be able to provide the correct redox properties, Lewis acidity, and electronic coordination capabilities (*52*, *58*), stringent requirements that we have confirmed cannot be fulfilled by Zn^{2+}.

CONCLUSIONS

The hypothesis of substoichiometric formation of the topaquinone cofactor in recombinant human diamine oxidase is substantiated by the crystal structure of the complex of a covalently bound high-affinity inhibitor aminoguanidine. The amount of mature cofactor correlates with the proportions of Cu^{2+} (active) and Zn^{2+} (inactive) ions at the active site as estimated by multiple-wavelength anomalous scattering measurements. Furthermore, this work structurally demonstrates, for the first time, that Zn^{2+} competes with Cu^{2+} directly for binding at the active site metal position.

ACKNOWLEDGMENT

We gratefully acknowledge Prof. David M. Dooley (University of Rhode Island, Kingston, RI) and Doreen Brown (Montana State University, Bozeman, MT) for the provision of purified human diamine oxidase used during the course of this work. We thank Dr. Megan Maher (The Centenary Institute, Sydney, Australia) for assistance with the collection of the X-ray diffraction data recorded at the Australian Synchrotron. Some of the data for this research were recorded on the MX2 beamline at the Australian Synchrotron.

REFERENCES

1. Schwelberger, H. G. (2004) Diamine oxidase (DAO) enzyme and gene. In Histamine: Biology and Medical Aspects (Falus, A., Ed.) pp 43−52, SpringMed Publishing, Budapest.
2. O'Sullivan, J., Unzeta, M., Healy, J., O'Sullivan, M. I., Davey, G., and Tipton, K. F. (2004) Semicarbazide-sensitive amine oxidases: Enzymes with quite a lot to do. *Neurotoxicology 25*, 303–315.
3. Sundaresan, M., Yu, Z. X., Ferrans, V. J., Irani, K., and Finkel, T. (1995) Requirement for generation of H_2O_2 for platelet-derived growth factor signal transduction. *Science 270*, 296–299.
4. Koskinen, K., Vainio, P. J., Smith, D. J., Pihlavisto, M., Yla-Herttuala, S., Jalkanen, S., and Salmi, M. (2004) Granulocyte transmigration through the endothelium is regulated by the oxidase activity of vascular adhesion protein-1 (VAP-1). *Blood 103*, 3388–3395.
5. Kaitaniemi, S., Elovaara, H., Gron, K., Kidron, H., Liukkonen, J., Salminen, T., Salmi, M., Jalkanen, S., and Elima, K. (2009) The unique substrate specificity of human AOC2, a semicarbazide-sensitive amine oxidase. *Cell. Mol. Life Sci. 66*, 2743–2757.
6. Best, C. H. (1929) The disappearance of histamine from autolysing lung tissue. *J. Physiol. 67*, 256–263.
7. Elmore, B. O., Bollinger, J. A., and Dooley, D. M. (2002) Human kidney diamine oxidase: Heterologous expression, purification, and characterization. *J. Biol. Inorg. Chem. 7*, 565–579.
8. Klocker, J., Matzler, S. A., Huetz, G. N., Drasche, A., Kolbitsch, C., and Schwelberger, H. G. (2005) Expression of histamine degrading enzymes in porcine tissues. *Inflammation Res. 54* (Suppl. 1), S54–S57.
9. Schwelberger, H. G., Hittmair, A., and Kohlwein, S. D. (1998) Analysis of tissue and subcellular localization of mammalian diamine oxidase by confocal laser scanning fluorescence microscopy. *Inflammation Res. 47*, S60–S61.
10. Bieganski, T., Kusche, J., Lorenz, W., Hesterberg, R., Stahlknecht, C. D., and Feussner, K. D. (1983) Distribution and properties of human intestinal diamine oxidase and its relevance for the histamine catabolism. *Biochim. Biophys. Acta 756*, 196–203.
11. Raithel, M., Kufner, M., Ulrich, P., and Hahn, E. G. (1999) The involvement of the histamine degradation pathway by diamine oxidase in manifest gastrointestinal allergies. *Inflammation Res. 48* (Suppl. 1), S75–S76.
12. Maintz, L., and Novak, N. (2007) Histamine and histamine intolerance. *Am. J. Clin. Nutr. 85*, 1185–1196.

13. Maintz, L., Schwarzer, V., Bieber, T., van der Ven, K., and Novak, N. (2008) Effects of histamine and diamine oxidase activities on pregnancy: A critical review. *Hum. Reprod. Update 14*, 485–495.
14. Holinka, C. F., and Gurpide, E. (1984) Diamine oxidase activity in human decidua and endometrium. *Am. J. Obstet. Gynecol. 150*, 359–363.
15. McGrath, A. P., Hilmer, K. M., Collyer, C. A., Dooley, D. M., and Guss, J. M. (2010) A new crystal form of human diamine oxidase. *Acta Crystallogr. F66*, 137–142.
16. McGrath, A. P., Hilmer, K. M., Collyer, C. A., Shepard, E. M., Elmore, B. O., Brown, D. E., Dooley, D. M., and Guss, J. M. (2009) Structure and Inhibition of Human Diamine Oxidase. *Biochemistry 48*, 9810–9822.
17. Dooley, D. M. (1999) Structure and biogenesis of topaquinone and related cofactors. *J. Biol. Inorg. Chem. 4*, 1–11.
18. Suzuki, S., Okajima, T., Tanizawa, K., and Mure, M. (2009) Cofactors of Amine Oxidases: Copper Ion and Its Substitution and the 2,4,5-Trihydroxylphenylalanine Quinone. In Copper Amine Oxidases: Structures, Catalytic Mechanisms and Role in Pathophysiology (Floris, G., and Mondovi, B., Eds.) pp 19−37, Taylor and Francis, Boca Raton, FL.
19. Duff, A. P., Cohen, A. E., Ellis, P. J., Hilmer, K., Langley, D. B., Dooley, D. M., Freeman, H. C., and Guss, J. M. (2006) The 1.23 Angstrom structure of *Pichia pastoris* lysyl oxidase reveals a lysine-lysine cross-link. *Acta Crystallogr. D62*, 1073–1084.
20. Langley, D. B., Trambaiolo, D. M., Duff, A. P., Dooley, D. M., Freeman, H. C., and Guss, J. M. (2008) Complexes of the copper-containing amine oxidase from *Arthrobacter globiformis* with the inhibitors benzylhydrazine and tranylcypromine. *Acta Crystallogr. 64*, 577–583.
21. Wilmot, C. M., Murray, J. M., Alton, G., Parsons, M. R., Convery, M. A., Blakeley, V., Corner, A. S., Palcic, M. M., Knowles, P. F., McPherson, M. J., and Phillips, S. E. (1997) Catalytic mechanism of the quinoenzyme amine oxidase from *Escherichia coli*: Exploring the reductive half-reaction. *Biochemistry 36*, 1608–1620.
22. Wilmot, C. M., Hajdu, J., McPherson, M. J., Knowles, P. F., and Phillips, S. E. (1999) Visualization of dioxygen bound to copper during enzyme catalysis. *Science 286*, 1724–1728.
23. Chen, Z., Schwartz, B., Williams, N. K., Li, R., Klinman, J. P., and Mathews, F. S. (2000) Crystal structure at 2.5 A resolution of zinc-substituted copper amine oxidase of *Hansenula polymorpha* expressed in *Escherichia coli*. *Biochemistry 39*, 9709–9717.
24. Crabbe, M. J., Childs, R. E., and Bardsley, W. G. (1975) Time-dependent inhibition of diamine oxidase by carbonyl-group reagents and urea. *Eur. J. Biochem. 60*, 325–333.
25. Padiglia, A., Medda, R., Lorrai, A., Murgia, B., Pedersen, J. Z., Finazzi Agro, A., and Floris, G. (1999) Interaction of Pig Kidney and Lentil Seedling Copper-Containing Amine Oxidases with Guanidinium Compounds. *J. Enzyme Inhib. 15*, 91–100.
26. Tamura, H., Horiike, K., Fukuda, H., and Watanabe, T. (1989) Kinetic studies on the inhibition mechanism of diamine oxidase from porcine kidney by aminoguanidine. *J. Biochem. 105*, 299–306.
27. Strange, R. W., Antonyuk, S. V., Hough, M. A., Doucette, P. A., Valentine, J. S., and Hasnain, S. S. (2006) Variable metallation of human superoxide dismutase: Atomic resolution crystal structures of Cu-Zn, Zn-Zn and as-isolated wild-type enzymes. *J. Mol. Biol. 356*, 1152–1162.
28. Szutowicz, A., Kobes, R. D., and Orsulak, P. J. (1984) Colorimetric Assay for Monoamine Oxidase in Tissues Using Peroxidase and 2,2′-Azinodi(3-ethylbenzthiazoline-6-sulfonic acid) as Chromogen. *Anal. Biochem. 138*, 86–94.
29. Leslie, A. G. W. (1992) Recent changes to the MOSFLM package for processing film and image plate data. *Joint CCP4+ESF-EAMCB Newsletter on Protein Crystallography,* 26.
30. Collaborative Computational Project Number 4 (1994) The CCP4 suite: Programs for protein crystallography. *Acta Crystallogr. D50*, 760–763.
31. Murshudov, G. N., Vagin, A. A., and Dodson, E. J. (1997) Refinement of macromolecular structures by the maximum-likelihood method. *Acta Crystallogr. D53*, 240–255.
32. Emsley, P., and Cowtan, K. (2004) Coot: Model-building tools for molecular graphics. *Acta Crystallogr. D60*, 2126–2132.
33. Schuttelkopf, A. W., and van Aalten, D. M. (2004) PRODRG: A tool for high-throughput crystallography of protein-ligand complexes. *Acta Crystallogr. D60*, 1355–1363.
34. Davis, I. W., Leaver-Fay, A., Chen, V. B., Block, J. N., Kapral, G. J., Wang, X., Murray, L. W., Arendall, W. B., Snoeyink, J., Richardson, J. S., and Richardson, D. C. (2007) MolProbity: All-atom contacts and structure validation for proteins and nucleic acids. *Nucleic Acids Res. 35*, W375–W383.
35. Otwinowski, Z., and Minor, W. (1997) Processing of X-ray diffraction data collected in oscillation mode. *Methods Enzymol. 276*, 307–326.
36. Smith, M. A., Pirrat, P., Pearson, A. R., Kurtis, C. R., Trinh, C. H., Gaule, T. G., Knowles, P. F., Phillips, S. E., and McPherson, M. J. (2010) Exploring the roles of the metal ions in *Escherichia coli* copper amine oxidase. *Biochemistry 49*, 1268–1280.
37. Mure, M., Brown, D. E., Saysell, C., Rogers, M. S., Wilmot, C. M., Kurtis, C. R., McPherson, M. J., Phillips, S. E., Knowles, P. F., and Dooley, D. M. (2005) Role of the interactions between the active site base and the substrate Schiff base in amine oxidase catalysis. Evidence from structural and spectroscopic studies of the 2-hydrazinopyridine adduct of *Escherichia coli* amine oxidase. *Biochemistry 44*, 1568–1582.
38. Mure, M., Kurtis, C. R., Brown, D. E., Rogers, M. S., Tambyrajah, W. S., Saysell, C., Wilmot, C. M., Phillips, S. E., Knowles, P. F., Dooley, D. M., and McPherson, M. J. (2005) Active site rearrangement of the 2-hydrazinopyridine adduct in *Escherichia coli* amine oxidase to an azo copper(II) chelate form: A key role for tyrosine 369 in controlling the mobility of the TPQ-2HP adduct. *Biochemistry 44*, 1583–1594.
39. Schuler, W. (1952) [The inhibition of histaminase]. *Experientia 8*, 230–232.
40. Holt, A. (2009) Membrane-Bound Copper Amine Oxidases. In Copper Amine Oxidases: Structures, Catalytic Mechanisms and Role in Pathophysiology (Floris, G., and Mondovi, B., Eds.) pp 69−101, Taylor and Francis, Boca Raton, FL.
41. Holt, A., and Baker, G. B. (1995) Metabolism of agmatine (clonidine-displacing substance) by diamine oxidase and the possible implications for studies of imidazoline receptors. *Prog. Brain Res. 106*, 187–197.
42. Burkard, W. P., Gey, K. F., and Pletscher, A. (1960) Inhibition of diamine oxidase in vivo by hydrazine derivatives. *Biochem. Pharmacol. 3*, 249–255.
43. Shore, P. A., and Cohn, V. H., Jr. (1960) Comparative effects of monoamine oxidase inhibitors on monoamine oxidase and diamine oxidase. *Biochem. Pharmacol. 5*, 91–95.
44. Sattler, J., and Lorenz, W. (1990) Intestinal diamine oxidases and enteral-induced histaminosis: Studies on three prognostic variables in an epidemiological model. *J. Neural Transm., Suppl. 32*, 291–314.
45. Thornalley, P. J. (2003) Use of aminoguanidine (Pimagedine) to prevent the formation of advanced glycation endproducts. *Arch. Biochem. Biophys. 419*, 31–40.
46. Abdel-Rahman, E., and Bolton, W. K. (2002) Pimagedine: A novel therapy for diabetic nephropathy. *Expert Opin. Invest. Drugs 11*, 565–574.
47. Freedman, B. I., Wuerth, J. P., Cartwright, K., Bain, R. P., Dippe, S., Hershon, K., Mooradian, A. D., and Spinowitz, B. S. (1999) Design and baseline characteristics for the aminoguanidine clinical trial in overt type 2 diabetic nephropathy (ACTION II). *Controlled Clin. Trials 20*, 493–510.
48. Peter, C., Laliberte, J., Beaudoin, J., and Labbe, S. (2008) Copper distributed by Atx1 is available to copper amine oxidase 1 in *Schizosaccharomyces pombe*. *Eukaryotic Cell 7*, 1781–1794.
49. Laliberte, J., and Labbe, S. (2006) Mechanisms of copper loading on the *Schizosaccharomyces pombe* copper amine oxidase 1 expressed in *Saccharomyces cerevisiae*. *Microbiology 152*, 2819–2830.
50. Cai, D., Williams, N. K., and Klinman, J. P. (1997) Effect of metal on 2,4,5-trihydroxyphenylalanine (topa) quinone biogenesis in the *Hansenula polymorpha* copper amine oxidase. *J. Biol. Chem. 272*, 19277–19281.
51. Takahashi, K., and Klinman, J. P. (2006) Relationship of stopped flow to steady state parameters in the dimeric copper amine oxidase from *Hansenula polymorpha* and the role of zinc in inhibiting activity at alternate copper-containing subunits. *Biochemistry 45*, 4683–4694.
52. Okajima, T., Kishishita, S., Chiu, Y. C., Murakawa, T., Kim, M., Yamaguchi, H., Hirota, S., Kuroda, S., and Tanizawa, K. (2005) Reinvestigation of metal ion specificity for quinone cofactor biogenesis in bacterial copper amine oxidase. *Biochemistry 44*, 12041–12048.
53. Brazeau, B. J., Johnson, B. J., and Wilmot, C. M. (2004) Copper-containing amine oxidases. Biogenesis and catalysis; a structural perspective. *Arch. Biochem. Biophys. 428*, 22–31.
54. Dove, J. E., Schwartz, B., Williams, N. K., and Klinman, J. P. (2000) Investigation of spectroscopic intermediates during copper-binding and TPQ formation in wild-type and active-site mutants of a copper-containing amine oxidase from yeast. *Biochemistry 39*, 3690–3698.
55. Schwartz, B., Dove, J. E., and Klinman, J. P. (2000) Kinetic analysis of oxygen utilization during cofactor biogenesis in a copper-containing amine oxidase from yeast. *Biochemistry 39*, 3699–3707.
56. Kim, M., Okajima, T., Kishishita, S., Yoshimura, M., Kawamori, A., Tanizawa, K., and Yamaguchi, H. (2002) X-ray snapshots of quinone

cofactor biogenesis in bacterial copper amine oxidase. *Nat. Struct. Biol. 9*, 591–596.
57. Wilce, M. C., Dooley, D. M., Freeman, H. C., Guss, J. M., Matsunami, H., McIntire, W. S., Ruggiero, C. E., Tanizawa, K., and Yamaguchi, H. (1997) Crystal structures of the copper-containing amine oxidase from *Arthrobacter globiformis* in the holo and apo forms: Implications for the biogenesis of topaquinone. *Biochemistry 36*, 16116–16133.
58. Samuels, N. M., and Klinman, J. P. (2005) 2,4,5-Trihydroxyphenylalanine quinone biogenesis in the copper amine oxidase from *Hansenula polymorpha* with the alternate metal nickel. *Biochemistry 44*, 14308–14317.
59. Weiss, M. S. (2001) Global indicators of X-ray data quality. *J. Appl. Crystallogr. 34*, 130–135.
60. Cruickshank, D. W. J. (1999) Remarks about protein structure precision. *Acta Crystallogr. D55*, 583–601.